Chapter 4
Investigating the Interphase in Hydroxyl-Terminated Polybutadiene (HTPB) Composites via Dynamic Mechanical Analysis and Atomic Force Microscopy

Jarred G. Tramell, Emily K. Hockey, Marcel M. Hatter, and Jesus O. Mares

Abstract State of the art explosive and propellant systems typically consist of energetic particles and a binder system. Specialized systems may contain additional components to meet application requirements, but in general these systems can be classified as highly filled polymer composite materials. The most extensively used binder systems across the energetics community are hydroxyl-terminated polybutadienes (HTPB). The HTPB binder functions to hold the particulates together into a consolidated structural media. It is well established that HTPB binders can significantly influence mechanical behavior, but much of the understanding of the fundamental mechanisms at play is lacking. Specifically, there exists a knowledge gap for the role of the interphase between the particles and the binder (i.e. the transition zone between pure binder and a particulate).

Dynamic mechanical analysis (DMA) is a technique that may shed light on the quality of the particle-binder interphase. Many polymer composites exhibit what appear to be two independent relaxation mechanisms via DMA experiments. There is general agreement that the first relaxation mechanism correlates to the glass transition temperature of the bulk polymer, however there is debate of the cause of the second relaxation mechanism. One prominent suggestion is that the secondary relaxation mechanism is attributed to the significant presence of an interphase region.

In this work we systematically investigate the effects of an effective interphase region on the presence of the loss factor peaks as exhibited through DMA experimentation. Specifically, we vary glass bead particle size in a HTPB-based composite and compare the loss factor to the measured effective volume of the interphase via atomic force microscopy (AFM). This approach may prove useful to understand the interphase mechanisms at play in energetic systems which will lead to the ability to create materials with tailored bulk mechanical properties and mitigate mechanical failures.

Keywords Hydroxyl-Terminated Polybutadiene · Filled Composite · Interphase · Dynamic Mechanical Analysis · Atomic Force Microscopy

Introduction

Hydroxyl terminated polybutadiene (HTPB) systems are some of the most common polymer matrices used for insensitive highly filled energetic systems such as polymer bonded explosives (PBX) and rocket propellants. HTPBs used in energetics typically consist of a crosslinked HTPB elastomer, plasticizer, and various stabilizers. The polymer matrix used in energetic systems is often described as the "binder" and primarily functions to (1) hold the particulates together into a consolidated structural media, (2) provide mechanical integrity to the system during loading scenarios and (3) reduce sensitivity of the energetic particles to mechanical stimuli.

In general, the interface between a particulate and the polymer matrix in filled composites creates an interphase region. This interphase region can be split into an inner layer and an outer layer. The inner layer contains polymer chains that are less

Jarred G. Tramell · Emily K. Hockey · Jesus O. Mares
Air Force Research Laboratory
e-mail: jarred.tramell.1@us.af.mil; emily.hockey.ctr@us.af.mil; jesus.mares.2@us.af.mil

Marcel M. Hatter
University of Dayton Research Institute, Eglin Air Force Base, FL 32542
e-mail: marcel.hatter.ctr@us.af.mil

Karen Kasza et al. (eds.), *Mechanics of Biological Systems and Materials and the Mechanics of Composite, Hybrid & Multifunctional Materials, Vol. 3*, Conference Proceedings of the Society for Experimental Mechanics Series, https://doi.org/10.13052/97887-438-0829-9_4

mobile than the bulk binder due to interaction with the particulate (i.e. tightly bound). The outer layer has higher mobility than the inner layer, but still less than that of the bulk binder (i.e. loosely bound). The reduction in molecular mobility and the sizes of the respective interphase regions depends on the polymer matrix used, and the particle's surface chemistry, volume fraction, particle size, particle size distribution, and quality of dispersion within the binder [1].

It is understood that the polymer matrix influences the overall mechanical behavior of the composite, but there is a lack of understanding of the how the interphase region between the HTPB binder and filler contribute to the overall mechanical behavior. Dynamic mechanical analysis (DMA) is a technique that may provide insight into the properties of the interphase. DMA provides information of the viscoelastic properties of a material, and specifically in this study tan δ (i.e. loss factor) is investigated. The tan δ represents the ratio between a material's loss modulus (energy dissipation) and storage modulus (energy storage). The tan δ provides insights into a material's ability to dampen vibrations or absorb impacts. A peak in a tan δ trace indicates that the material is exhibiting a significant energy loss. This energy loss is primarily attributed to increased molecular mobility within the material and is often associated with a specific relaxation process (e.g. the glass transition temperature). In filled HTPB energetic systems, many have reported the presence of two distinct tan δ peaks, which suggests the presence of two distinct relaxation processes [2–6].

The first tan δ peak at the coldest temperature is broadly accepted to describe the glass transition temperature (T_g) of the bulk HTPB binder. However, there are several explanations of the origin of the second-broader tan δ peak that occurs at warmer temperatures. The second tan δ peak is commonly attributed to a separate relaxation process solely within the binder. The most frequent explanation attributes the second peak to the hard and soft segments of the HTPB binder. Another explanation ascribes this to the presence of sol-gel content in the polymer network (i.e. non-crosslinked chains) [3–5]. Despite previously published explanations for the additional tan δ peak in filled HTPB systems, other filled composite systems often link this second peak to the presence of an interphase region [1]. Although not universally applicable to every filled system, the interphase relaxation mechanism seen in DMA data for many other systems warrants consideration as the underlying mechanism of the second tan δ peak in highly filled HTPB systems [1, 7–9].

Bashir discusses several alternative and complimentary approaches to DMA that other investigators have used to characterize the interphase region such as nuclear resonance spectroscopy (NMR), atomic force microscopy (AFM), Raman spectroscopy, and dielectric relaxation spectroscopy [1]. AFM is perhaps the most attractive option since the technique can measure the widths and modulus of the interphase regions and could be useful to correlate interphase characteristics to tan δ peak heights and widths from DMA data.

The selected approach of this work is to systematically change the particle size of filler and modify the particles' surface chemistry, both of which should change the volume fraction of interphase region [1]. Changes to the effective interphase volume are expected to create changes in DMA tan δ traces and AFM measurements. By pairing DMA and AFM measurements, it may be possible to determine if DMA can infer additional information on the interphase region in filled HTPB systems (e.g. the interphase size).

Materials

A typical HTPB binder system was selected as the polymer matrix. Table 1 summarizes the components of the HTPB system. Soda-lime silica glass spheres (glass beads) were selected as the filler instead of energetic particles to simplify testing logistics and estimation of total surface area of the solids in the system. The weight percent of glass beads was chosen to generate a system with 50 volume % of filler. The filler content for all mixes was fixed at 50 volume % and the sizes of the glass beads were varied.

Table 1 Filled HTPB composition

Ingredient	Function	Weight %
Poly bd® R45 HTLO	Prepolymer	18.41
Isodecyl pelargonate (IDP)	Plasticizer	6.138
Dibutyltin dilaurate (DBTDL)	Catalyst	0.04242
Ethyl 702	Antioxidant	0.1564
Isophorone diisocyanate (IPDI)	Curative	1.766
Soda-lime silica glass sphere	Filler	73.49

Soda-lime silica glass should have a high level of interaction with the binder due to the surface silanol groups at the beads' surface. The silanol groups can react with the IPDI and create a covalent bond between the filler and the polymer network.

To tune the surface chemistry of the glass beads, Sigmacote® was applied to the particles. Sigmacote® is a siliconizing reagent for glass and is intended to function in this system as a shielding agent to reduce particle-binder interaction effects and prevent particle-binder covalent bonding. Glass beads were purchased from Potter's Industries and Sigmacote® was purchased from Sigma-Aldrich. Mixes were generated with and without coated glass beads in this work. For the remainder of this study, mixes that utilize glass beads with Sigmacote® are denoted with the suffix "-SC".

Prior to mixing, glass beads were sieved to reduce the span of the particle size distribution. The grades of spheres selected in this work and the U.S. mesh sieves that the beads were collected between are shown in table 2. Table 2 also includes particle size data on the post processed glass beads. The particle size data confirms that the application of Sigmacote® did not significantly change the particle size distributions of the glass beads.

Table 2 Particle size data and surface area estimates for coated and uncoated glass beads

Filler	U.S. Mesh	Dv10 (μm)	Dv50 (μm)	Dv90 (μm)	Average Particle Size (μm)	Surface Area per mL of filler (cm^2/mL)
P4000	325,500	7.14	21.26	39.70	14.35	4181
P4000-SC	325,500	8.78	23.42	41.15	16.75	3582
P0040	120,170	59.66	69.25	81.08	66.5	902.2
P0040-SC	120,170	55.97	68.64	86.4	67.64	530.0
P0080	70,80	151.4	178.0	207.5	176.4	340.1
P0080-SC	70,80	149.1	174.6	205.6	173.3	346.2
P0170	40,45	340.1	378.5	412.5	375.3	159.8
P0170-SC	40,45	331.2	375.1	411.0	370.8	161.8
P0280	25,30	529.9	608.7	680.5	602.0	99.67
P0280-SC	25,30	523.5	606.1	695.8	602.5	99.59

Formulation components were weighed out and hand-mixed for two minutes at ambient temperature. After hand-mixing, the mixture was degassed in a vacuum chamber at ambient temperature for 10 minutes to remove air in the system. Larger sphere sizes showed minimal settling at the end of the degassing step and were gently mixed to resuspend particles to mitigate settling and reintroduction of air. Mixes were then poured into open face 3.2 x 12.5 x 60 mm molds and cured at 60 °C for 48 hours. Qualitatively, no settling was observed by eye in the cured samples.

Figure 1 shows a picture of cured samples. A color difference is observed between the coated and uncoated beads. At this time, it is unknown what caused the color change. Some potential explanations could be as follows: side reactions/molecular complexing between the Ethyl 702 or DBTDL and Sigmacote®, or refractive index differences between glass beads with and without covalent bonding to the binder. Currently, we have dismissed residual HCl from the coating reaction as the root cause, as coated beads were washed with deionized water and the rinse had a neutral pH. The underlying cause of the color may have an inconsequential effect on the results, since color changes can manifest at ppm levels, but it cannot be discounted when interpreting the results.

Methods

Dynamic mechanical analysis

DMA data was collected with a TA Instruments Discovery Hybrid Rheometer (DHR20) equipped with a rectangular torsional geometry. Samples were tested with a frequency sweep (0.01, 0.1, 1, and 10 Hz) from -110 to 100 °C with 1°C temperature steps and a 0.1% oscillatory strain. Samples were verified to be within the linear viscoelastic regime (LVR) prior to selecting the 0.1% oscillatory strain. A tensile axial force of 0.15 ± 0.1 N was maintained throughout the procedure to avoid skewing results from thermal expansion/contraction. Specimens were equilibrated for 45 seconds prior to data collection at each temperature step. Collected DMA data is parsed into tan δ vs temperature curves at each respective test frequency (0.01, 0.1, 1, and 10 Hz) for analysis.

DMA data processing

Since DMA traces for filled HTPB composites historically exhibit two overlapping tan δ peaks, such as the example shown in figure 2, it is necessary to decompose the traces into distinct peaks to properly quantify the peak heights, widths, and areas.

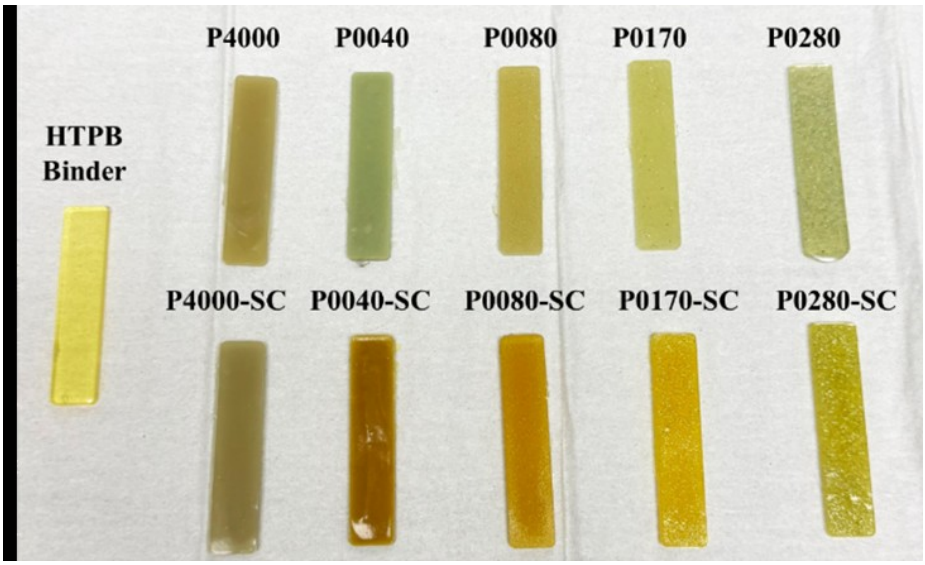

Fig. 1 Picture of cured DMA samples where the glass bead size increases from left to right and uncoated and coated beads are on the top and bottom of the image, respectively

Tsagaropoulos & Eisenberg first proposed modelling and decomposing tan δ traces with an exponential background and two exponentially modified Gaussian (EMG) distributions [9]. However, their approach has since been adapted By Cerri and Bohn towards HTPB systems which models tan δ traces with three EMG distributions to quantify the peak heights, widths, and areas [10]. To fit the tan δ traces to EMG curves, the data is baseline corrected then fitted to equation (1). Variables used in equation (1) are bulleted below with their associated units used. td_0 was set to zero for this work.

The effect of the glass bead particle size and coating on the parameters listed in equation (1) will be assessed. Any reduction in A_i is reported by Bohn *et. al*. to relate to the hindrance of molecular mobility in the system [4]. Additionally, the authors of this study speculate that larger w_i values correlate to a larger distribution of relaxation times and thus a larger interphase region.

$$\tan(\delta)_{BL} = td_0 + \sum_{i=1}^{N} \frac{A_i}{\tau_i} \bullet \frac{1}{2} \bullet exp\left[0.5 \bullet \left(\frac{w_i}{T_{0_i}}\right)^2 - \frac{T - T_{c_i}}{\tau_i}\right] \bullet \left\{1 - \text{erf}\left[-\frac{1}{\sqrt{2}} \bullet \left(\frac{T - T_{c_i}}{w_i} - \frac{w_i}{\tau_i}\right)\right]\right\} \quad (1)$$

- T - measurement temperature (K)
- $\tan(\delta)_{BL}$ - value of tan δ after baseline correction as a function of T (-)
- A_i - EMG peak areas (K)
- w_i - half width at half height of the gaussian peak (K)
- T_{c_i} – temperature at Gaussian peak maximum (K)
- τ_i - relaxation parameter in exponential part of EMG (K)
- td_0 – offset in tan δ data (-)
- N – number of EMG fitting functions

The values for T_{c_i} at each Gaussian peak are also used to calculate the activation energy (E_a) of each relaxation process with the Arrhenius equation (shown in equation 2) where f is the applied test frequency, f_0 is a pre-exponential factor, R is the ideal gas constant, and $T(f)$ is the temperature at a given tan δ peak at each deformation frequency (T_{c_i} in this case). Calculating the E_a will provide further insight of the interphase since higher activation energies indicate stronger particle-filler interactions [11, 12].

$$f = f_0 \bullet exp\left(-\frac{E_a}{R * T(f)}\right) \quad (2)$$

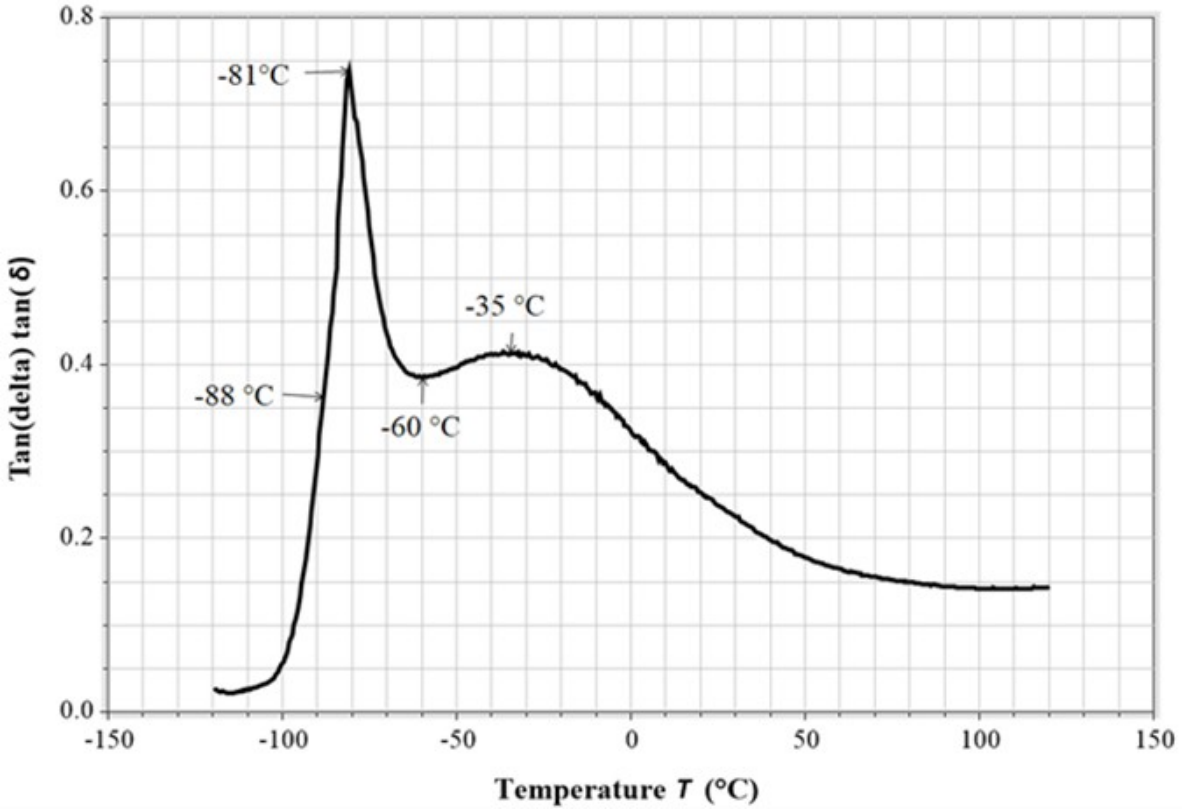

Fig. 2 Representative tan δ curve of filled HTPB composites [6]

Atomic force microscopy

AFM analysis was performed at room temperature (RT) and ambient pressures using a Jupiter XR AFM (Oxford Asylum Research) in the Fast Force Mapping (FFM) mode. Two cantilevers were used to investigate potential effects of a cantilever coating on the nanomechanical results. The AC160TS-R3 (uncoated lever) and the AC160TSA-R3 (lever coated with Cr/Au (5/65)) both consist of a 7 nm radius uncoated silicon tip, with a resonance frequency (f) of 300 (200–400) kHz and a spring constant (k) of 26 (8.4–7) N/m. Using this mode, the tip of the cantilever physically contacts the composite sample, allowing for nanomechanical information (such as adhesion and Young's modulus) to be derived in addition to standard topographical reconstruction of the surface. The total scan area for the present AFM images is 10 μm x 10 μm u, with individual line scans across a given interphase on a shorter scale (2-5 μm).

AFM sample preparation

For ideal measurements of the interphase using AFM, samples must be cross sectioned with extreme precision to expose a flat surface across the constituents [13–16]. Due to the highly compliant nature of HTPB binder, such uniform preparation has proven difficult to achieve with cryo-ultramicrotomy (see section 4.2 for discussion). Due to challenges cutting 73.49 wt. % loaded samples, all HTPB/glass bead composite samples for AFM analysis were 4.0 wt. % solids loading (1.5 volume %), nominally 25–40 μm size, with varied coating of the glass beads (uncoated or Sigmacote®). Each sample was razor cut to $\sim$ 5mm (length) $\times$ 1mm (width) for ease of mounting in the cryo-microtome (Leica EM FC7). These samples were then sectioned for AFM analysis using two different microtome blades. A tungsten carbide knife (Delaware Diamond Knifes) was used to expose the desired cross section, followed by a diamond knife (DiATOME, cryo-AFM) that used a 50–100 nm feed to act as a "polishing" step for a smooth surface. Both composite samples and knives were held at -140°C (below the T_g of the HTPB system, determined to be -84 ° at 0.01 Hz in this work) with liquid nitrogen throughout the entire cutting process before being quickly warmed to RT under a nitrogen purge to mitigate the accumulation of unwanted condensation on the sample surface. Finally, the composite samples were secured to a magnetic AFM specimen disc with carbon tape for analysis.

Results and Discussion

DMA results

An overlay of the tan δ traces collected at 1 Hz is shown in figure 3a–d. Peak position for the first tan δ peak generally did not change across all systems investigated, indicating there is no appreciable change in T_g from the addition of filler. This observation is consistent with other studies on different filled composite systems that vary filler content and particle size [1, 9]. However, Bashir summarizes results of others that have reported the opposite and the shift in T_g appears to be rooted in the interaction strength between the particle and filler, which in turn can create dependencies on filler content and particle size [1].

The results also show that there is a height reduction in the first tan δ peak from the introduction of filler. The literature strongly suggests that the height of the tan δ peak is dependent on the particle size. The smaller the particles are, the lower the resultant tan δ peak will be. This can be attributed to more interfacial adhesion from the increase in surface area of filler [17–20]. Additionally, the tan δ peak height is believed to be dependent on the strength of the interfacial interaction. Stronger interactions result in the larger reductions of the tan δ traces [1, 18, 20].

The peak height of the first tan δ peak is plotted vs average particle size in figure 4. The coated glass beads always exhibited a higher peak value than their uncoated counterpart, which suggests that the Sigmacote® effectively reduced the particle-binder interaction strength. However, the trends in particle size did not agree with the expectations discussed above. For both the coated and uncoated systems, figure 4 shows that that the peak height diminished from the P4000 beads until the P0080 beads followed by an increase. The uncoated P0280 also traced lower than the P0170 where as the P0280-SC traced higher than the P0170-SC as expected.

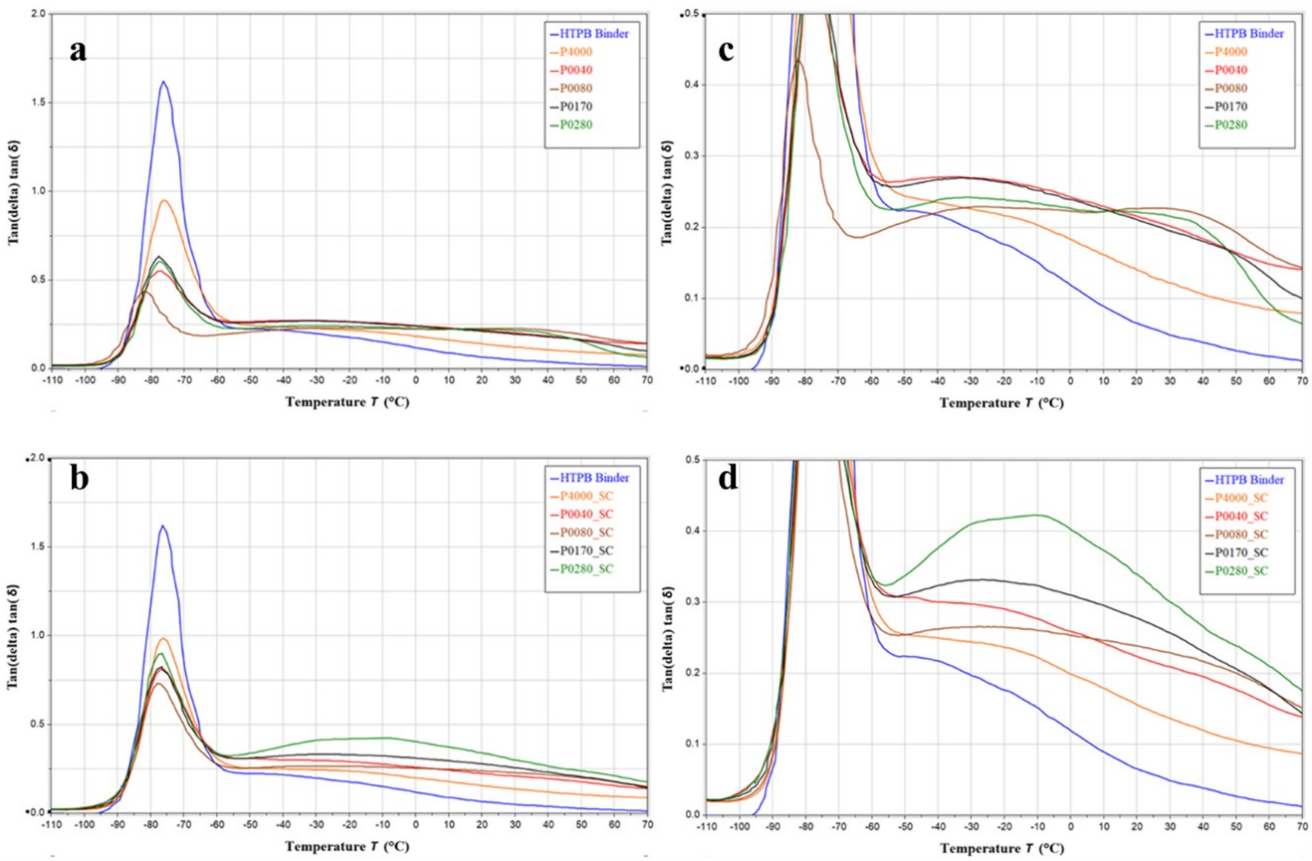

Fig. 3 1Hz tan δ vs temperature trace of HTPB binder and filled samples with **a)** uncoated glass beads and **b)** coated glass beads **c)** Rescaled tan δ vs temperature trace of uncoated glass beads **d)** Rescaled tan δ vs temperature trace of coated glass beads

One explanation for this unexpected behavior is the possible presence of agglomerates in the final samples. P4000, P4000-SC, P0040, and P0040-SC likely need longer and/or more aggressive mixing cycles to properly disperse the particles

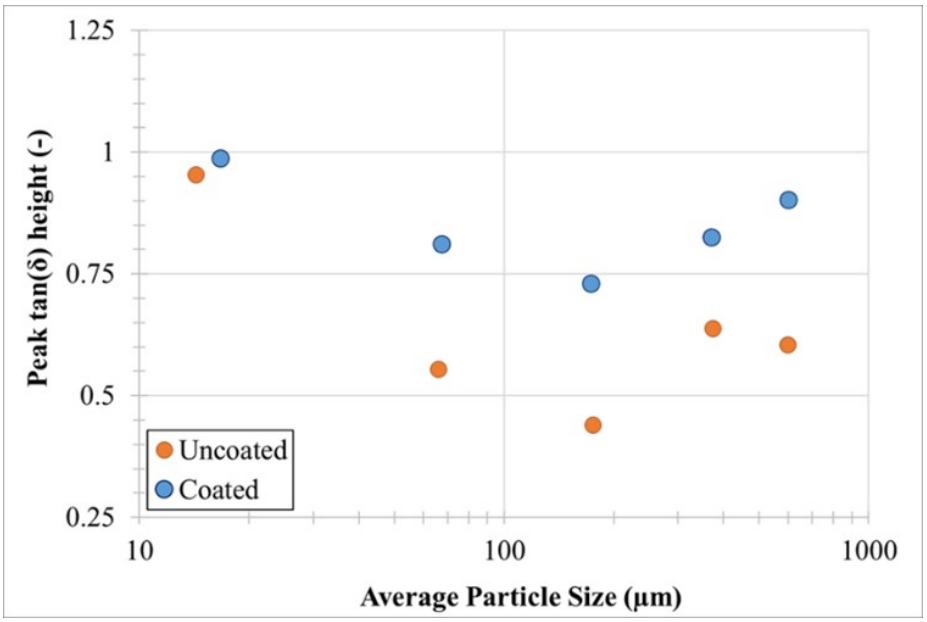

Fig. 4 Max tan δ height vs average particle size in HTPB/glass bead composites

in the binder. Without proper dispersion, a cluster of particles can effectively behave as a larger particle and reduce the overall surface area of the filler.

Additionally, not all samples exhibited a distinct secondary peak at warmer temperatures. Specifically, the P4000, P4000-SC, and P-0040-SC samples. With the suspected agglomeration issues, it is unknown if this is representative behavior or due to the lack of particle dispersion. The HTPB binder also appears to exhibit an underlying secondary tan δ peak. This suggests that there is a second relaxation process occurring in the binder alone, but it is impossible to determine if the introduction of filler affects the second relaxation process in the HTPB or creates a new relaxation process from creation of an interphase.

Furthermore, looking at the uncoated beads in figure 2b there is no clear trend in the trace heights above T_g. We would expect to see a correlation with particle size as discussed above, but any trends remain unclear even if the P4000 and P0040 samples are disregarded. However, a trend exists in the traces of the coated beads in figure 2d if sample P0040-SC is excluded. Sample P4000-SC is still suspected to be an outlier due to agglomeration concerns, but there appears to be a direct relationship between particle size and the height of the second tan δ peak as we should expect.

Comparing the coated and uncoated, the coated beads consistently exhibited a higher second tan δ peaks. The uncoated and coated P4000 and P0040 samples did not exhibit identifiable peaks, but the coated beads still showed higher tan δ traces beyond the T_g. Interestingly, it seems there is another tan δ peak for the P0280 and P0080 glass beads around 30 °C. The underlying cause is currently unknown but implies a potential third relaxation process for these systems.

EMG fitting

The tan δ curves were modelled after baseline correction with EMG functions shown in equation 1. The initial purpose of the EMG modelling was to quantify the peak heights, widths, and areas, and use T_{c_i} calculate the $E_a$of the relaxation processes. It was found that some systems could be modelled adequately with two EMG functions, while others required three. Optimization schemes for data sets requiring three EMG functions often yielded multiple analytical solutions for all parameters. Figure 5a shows an example of the range of EMG fitting solutions. Up to a 50 °C difference in T_{c_2} and T_{c_3}could occur when fits had multiple analytical solutions.

Additionally, some traces could be modelled adequately with two or three EMG functions as demonstrated in figure 5b. In these cases, the model with three EMG functions did not appear to accurately assign T_{c_2} to the second tan δ peak due to over fitting, but the models with two EMG function did. Lastly, most of the second tan δ peak height differences were erased with the baseline correction function that minimized differences for A_i between samples. Analysis of the EMG function parameters and T_{c_i} values for E_a calculations is not reported for reasons just mentioned.

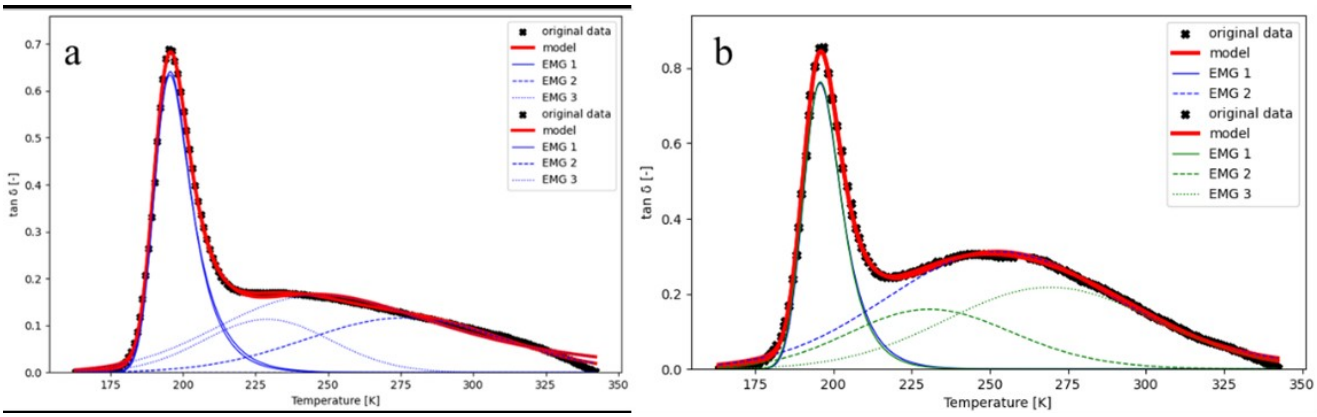

Fig. 5 **a)** Example of EMG model fit resulting in multiple analytical solutions for P0080-SC **b)** P0280-SC with fitted with two and three EMG functions

Activation energy calculations

Due to the issues with the EMG fitting, E_a calculations were completed with the peak heights directly from the tan δ traces rather than the T_{c_i}. Peak temperatures are reported in table 3 below. Values are not reported when a material or test condition did not result in any identifiable peaks. 10 Hz data is also not reported for the second tan δ peak due to phase angle issues with data above Tg. Strain % increases within the LVR can be employed in the future to mitigate this issue when testing above the binder T_g [4].

The results suggest that introduction of the filler increases the E_a of the bulk polymer T_g and the E_a of the second tan δ peak when comparing neat binder to all the filled samples. Looking specifically at the E_a for the T_g peak, no obvious trends exist between E_a and the filler particle size, or the E_a of coated vs uncoated beads. Data fitting for the second tan δ peak is relatively poor due to the lack of frequencies available. Including additional frequencies in future testing will allow more accurate E_a calculations. Despite the lack of data, there appears to be a difference between the E_a of coated and uncoated samples. Again, excluding P4000, P4000-SC, P0040, and P0040-SC samples, the remaining materials consistently exhibited a lower E_a in the coated glass beads vs the uncoated counterparts. The reduction in E_a indicates a weaker interaction with the binder [12].

Particle-binder interaction parameter

The particle-matrix interaction parameter, *A*, was first proposed by Chua and adapted by Kubat *et al.* [17, 20]. The equation provided by Kubat *et. al.* is shown in equation 3 and is based on the energy loss at the interface. In equation 3, v_f is the volume fraction of filler, and $tan\,(\delta_c)$ and $tan\,(\delta_m)$ are the composite tan δ and binder tan δ traces, respectively, as a function of temperature. The parameter *A* discussed here is different than the model parameter A_i discussed previously in equation 1. The parameter *A* has an inverse relationship with the polymer-filler interaction, meaning lower *A* values indicate a stronger particle-binder interaction. Calculations of the interaction parameter may shed light on interphase characteristics when coupled with AFM results.

$$A = \frac{1}{1 - v_f} \bullet \frac{tan\,(\delta_c)}{tan\,(\delta_m)} - 1 \tag{3}$$

The interaction parameter *A* is plotted vs temperature in figure 6 for the 1 Hz data sets. All samples follow a similar shape and can be generally broken down into three regimes. In the first regime, *A* increases slightly from -110 °C to -95 °C which indicates a weakening interaction strength as the temperature approaches T_g. Second, *A* decreases from -95 °C to the -75 °C (in the T_g range at 1 Hz) and may be attributed to increased molecular mobility in the binder which increases viscosity and friction at the interface [21, 22]. Third, *A* generally increases from -75 °C until the end of the test where the binder particle interaction decreases as molecular mobility continues to increase [21, 22]. Some samples show a decrease in *A* at warmer temperatures, with the P0280 samples showing a significant increase in the particle-binder interaction. The underlying mechanism for this decrease of *A* at warmer temperatures is currently unknown.

The difference in the *A* parameter between coated and uncoated glass beads is also apparent across all samples above their T_g. First, every coated sample shows a higher *A* parameter, again suggesting that the interaction strength is weaker than the uncoated counterpart. Next, looking at uncoated samples, the *A* parameter does not exhibit many differences across

Table 3 Activation Energy calculations for T_g and second tan δ peak

T_g (°C) values at each test frequency						
Sample	0.01 Hz	0.1 Hz	1 Hz	10 Hz	E_a (kJ/mol)	R^2
HTPB	-83.76	-80.25	-76.26	-70.75	169.16	0.993
P4000	-82.92	-79.9	-76.16	-71.15	186.46	0.991
P4000-SC	-82.98	-79.99	-75.98	-71.00	182.44	0.991
P0040	-85.16	-80.82	-76.99	-72.75	175.47	0.999
P0040-SC	-83.97	-81.03	-76.97	-71.96	179.84	0.991
P0080	-85.39	-81.95	-77.97	-73.58	181.70	0.999
P0080-SC	-84.07	-80.97	-77.94	-73.04	198.12	0.989
P00170	-85.07	-80.57	-77.69	-73.16	185.11	0.993
P0170-SC	-83.49	-81.47	-76.55	-71.89	179.22	0.976
P0280	-84.24	-81.03	-77.3	-72.09	179.19	0.991
P0280-SC	-84.09	-80.80	-76.79	-73.21	197.23	0.999
2^{nd} tan δ peak temperature (°C) at each test frequency						
Sample	0.01 Hz	0.1 Hz	1 Hz	10 Hz	Ea (kJ/mol)	R^2
HTPB	-58.77	-52.91	-45.13	-	136.66	0.996
P4000	-	-	-		-	-
P4000-SC	-50.9	-44.00	-		141.30	1.00
P0040	-40.52	-34.97	-35.82		279.28	0.621
P0040-SC	-52.03	-49.98	-48.05		478.58	0.999
P0080	-31.76	-26.85	-26.82		347.70	0.755
P0080-SC	-41.02	-35.03	-26.06		145.41	0.991
P00170	-38.7	-33.82	-31.97		300.37	0.934
P0170-SC	-35.28	-32.32	-26.95		262.63	0.976
P0280	-38.36	-35	-31.97		338.81	0.999
P0280-SC	-30.05	-27.79	-10.39		104.59	0.841

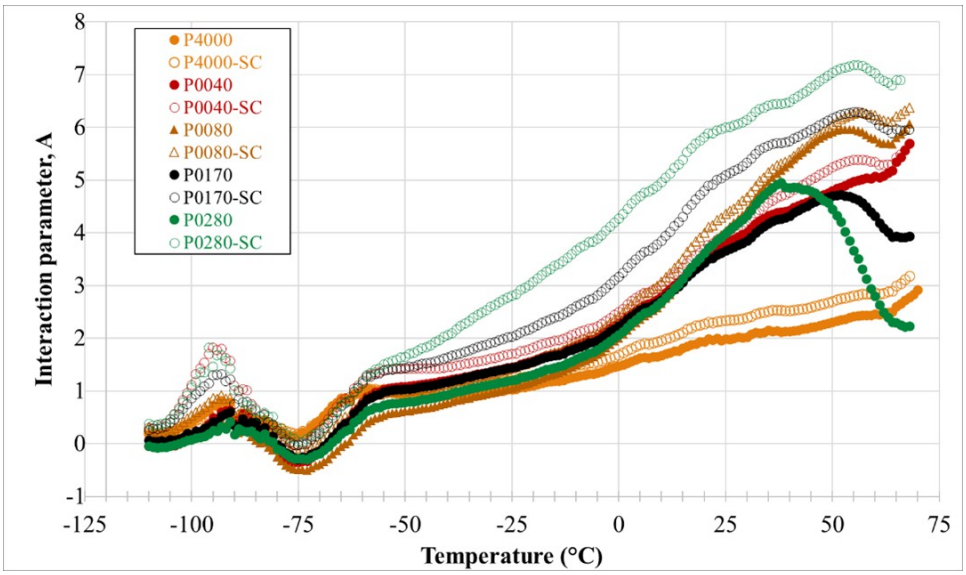

Fig. 6 Interaction parameter *A* vs temperature where parameter *A* has an inverse relationship with particle-binder interfacial strength

particle sizes until approximately -10 °C, where the P4000 sample continues increasing at the same slope, and all other samples exhibit a slope increase. There are not many differences between the P0040, P0080, P0170, and P0280 samples until they exhibit their respective decreases at warmer temperatures.

Finally, examining the coated samples, all samples have a similar *A* parameter below T_g, but distinct differences emerge above T_g. Smaller coated particles generally showed lower *A* values than the larger coated particles. Samples also displayed an inverse relationship between the slope of the *A* parameter above T_g. This implies that smaller particles experience higher particle-binder interactions and are not as sensitive to changes in the interaction at temperatures above T_g. While the larger particles see a faster increase in the *A* parameter across temperature increases.

Other approaches are available to calculate various interaction parameters or specific activation energies of the interphase. However, all these approaches require systematic changes in the volume % to calculate these values [11, 23]. This type of data is not available yet for this work but may serve as an alternative in the future to characterize interphase properties via DMA.

AFM Results

Highly loaded and/or large particle sized glass bead samples, as used in the DMA experiments, were found to pose a great risk of damaging the microtome knives, thus damaging the binder and causing large variation in height between constituents. During initial attempts to microtome samples with P0280 glass beads (602 μm average particle size), the tungsten carbide knife chipped and was unable to section the bead. In an attempt to preserve the knives operational life, only smaller glass bead sizes were used moving forward. Figure 7 shows an optical image of the surface of the 50 volume % P4000 sample prepared via cryo-microtome. Although the glass beads were cut in half, the binder remains rough and damaged—visualized as unfocused optically, opaque, no discernable features that result from cutting (seen as elongated strides on the glass beads)—which is likely result of a damaged/dull knife unable to section the sample surface properly. To increase the cut quality and protect the knives from further damage, 4 wt. % particle loadings were used as they minimize the frequency of particle contacts with the knife.

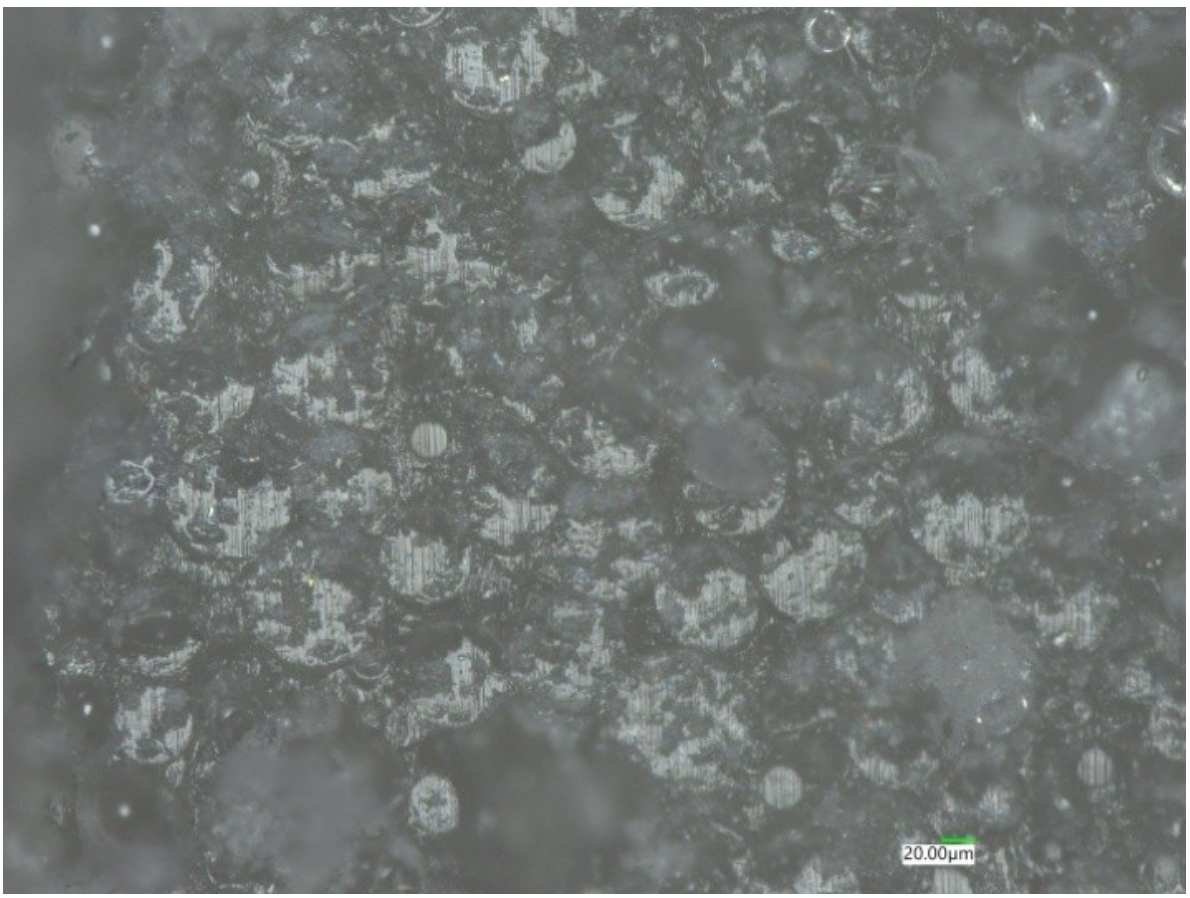

Fig. 7 Optical image of the surface of sample P4000 sample at 50 volume % solids loading prepared via cryo-microtome

When the knives did not sustain appreciable damage during the cutting process, cutting thin slices from the surface was used to mitigate large variations in height across the surface and between constituents. However, when the binder is as

compliant as HTPB and must be cooled to section, another consequence arose. We observe that the embedded particle—having the appearance a pristine flat cut optically at cryogenic temperatures—appeared to be protruding from the binder once the sample was brought to RT (see the top (red) trace of figure 8 for reference). We believe this phenomenon is a direct result of HTPB's relatively large coefficient of thermal expansion to that of soda-lime silica glass of HTPB as it warms to RT, thus altering the prepared surface [24]. Other surface preparation approaches—cryo- and RT hand polishing and cryo- and RT broad beam ion milling—have been attempted to overcome this unforeseen consequence. For each mitigation strategy, we observe issues. Particle pull out (from hand polishing), charring of the HTPB (from ion milling), and metal re-deposition (from ion milling) significantly alter the surface and, in turn, irreversibly alter the interphase. At the time of this study, we are continuing to investigate other cross sectioning techniques (such as oscillating diamond knives, diamond wire saw, etc.) that will not induce damage and minimize the observed thermal expansion issue, while still preparing a flat surface for high quality AFM measurements.

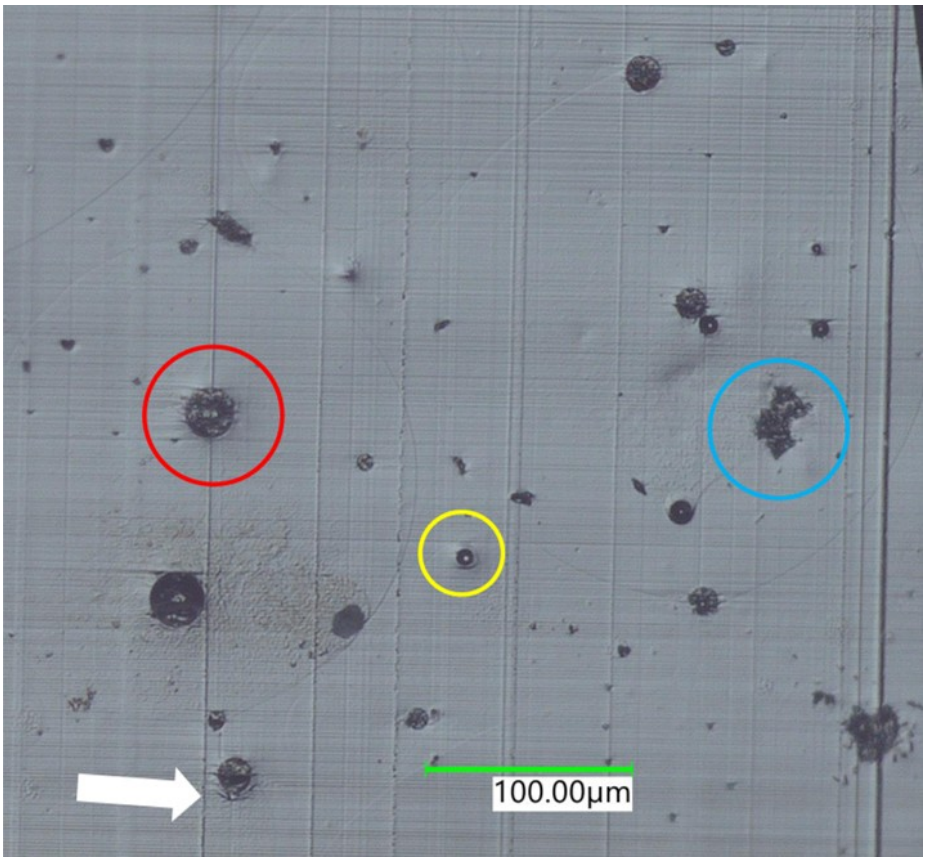

Fig. 8 Optical image of the surface of P4000 (4 wt. %) composite sample prepared via cryo-microtome. Cutting direction is from top to bottom of the image. Elongated vertical lines running through the sample are knife marks, an artifact based on knife damage. Colored circles and arrow highlight interesting features of the cross section, see main text

Figure 8 shows a representative optical image of the cryo-microtome P4000 (4 wt. %) surface used for AFM analysis. We note key features of the cross sectioned surface to highlight the difficulties of sample preparation, and the obstacles faced in finding a viable bead/interphase to analyze. The cutting direction is from top to bottom of the image. The red circle in figure 8 shows a glass bead that is cut in half (and appears slightly raised from the HTPB binder) but does not exhibit the same knife marks as the surrounding HTPB sample (elongated vertical lines). Such an artifact can be indicative of a fractured glass bead instead of one that is cleanly cut. Highlighted in yellow in figure 8, we observe a vacancy in the HTPB where a glass bead was pulled out of the sample. The blue circle in figure 8 highlights a conglomerate of smaller glass beads that presents as a non-spherical cluster. Finally, we can observe a 'lip' behind some of the embedded beads (shown with the white arrow in figure 8) that correlates with the 'back' of the bead in terms of cutting direction. All of these artifacts allude to damage imparted by the cutting process, which will likely affect the measured interphase width.

Nevertheless, we attempt AFM analysis on coated and uncoated P4000 composites at 4 wt. % loading. Two glass beads were identified in the P4000-SC sample and are denoted as bead A and bead B. Two glass beads are also identified in the

P4000 sample and denoted as beads C and D. The nanomechanical properties of a sample measured using AFM consist of the height, adhesion, and Young's modulus. These properties can be presented in two configurations, as shown in figure 9 as 3D/2D color map images and figure 10 as a plot. For the AFM analysis herein, we define adhesion as the force needed to disengage the tip of the cantilever from the surface of the sample and the Young's modulus as the measure of the sample's resistance to elastic deformation under a given load, calculated using the known tip geometry of the selected cantilever and assuming Hertzian contact mechanics. The adhesion and Young's modulus values reported are relative rather than absolute because 1) it is historically difficult to validate such analytical approach across constitutes of drastically different properties and height and 2) the main goal of AFM analysis is to measure the width of the interphase (a measure of how far, moving away from the glass bead, until the binder properties are representative of the bulk).

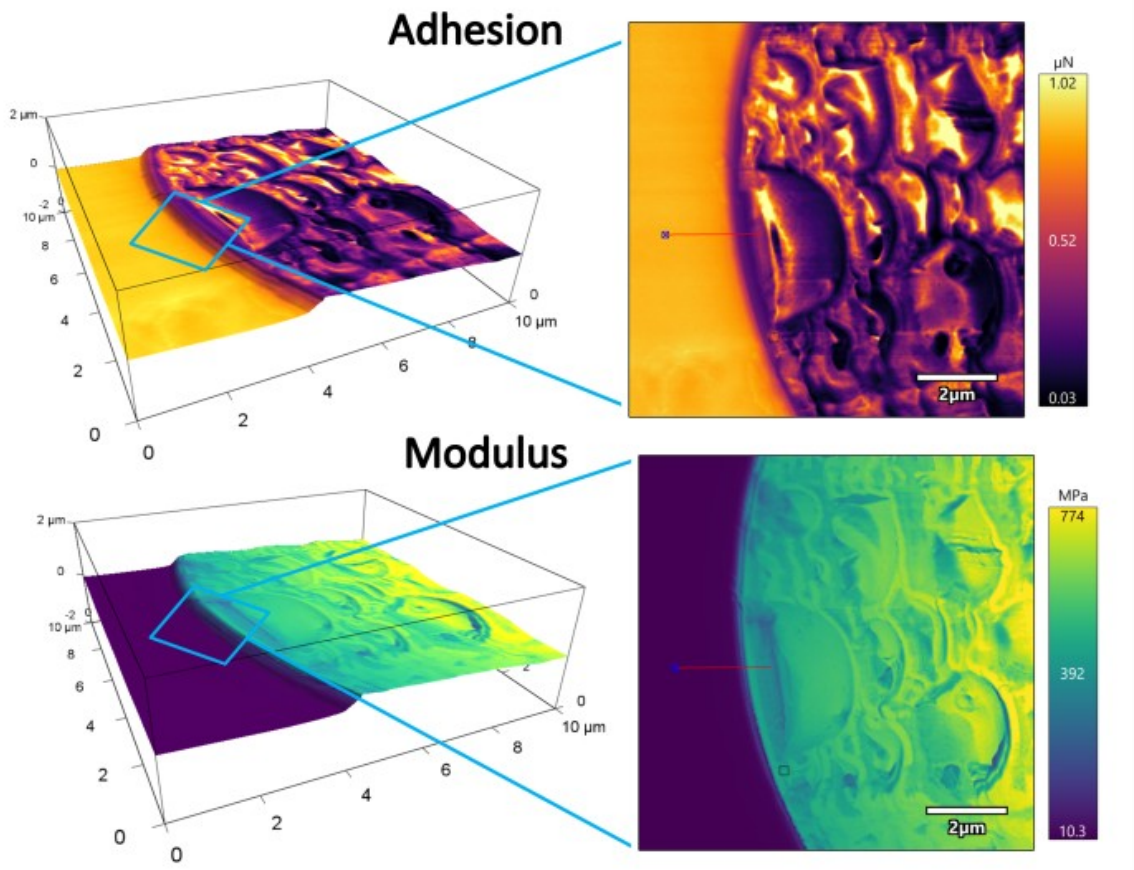

Fig. 9 3D images of P4000-SC (∼30 µm, bead A) sample topography (left) obtained over a 10 µm × 10 µm FFM scan overlaid with a color map representing the adhesion (top, Inferno color map) and Young's modulus (bottom, Viridis color map). 2D zoomed-in images (right) of adhesion (top) and modulus (bottom) interphase, where the solid red line represents the line scan across the interphase. The HTPB binder is on the left side of each image and the glass bead is on the right side

Highlighted in Collinson et al. 2021 (and references therein), changes in sample height can induce non-ideal tip-surface interactions that can in turn lead to 'dead-zones' where the information gathered becomes non-quantitative [14]. It is extremely difficult to detangle whether the sudden change in height causes the change in nanomechanical properties, or if the sudden change in nanomechanical properties causes artifacts in the topography resulting from different indentation depths. Acknowledging the likelihood of dead-zones that could result from non-flat surface preparation, we report tentative interphase widths as we continue to investigate best practices and mitigate undesirable artifacts of multi-component systems with starkly different properties.

The 3D images (figure 9, left) visualize the topography of a given binder/bead region (bead A) of a P4000-SC sample across a 10 µm × 10 µm scan area, overlaid with the adhesion (figure 9, top panel) or Young's modulus (figure 9, bottom) information. The 2D images (figure 9, right) represent a smaller portion of the sample surface, more easily depicting the color gradient moving from the bulk HTPB (represented as orange in the adhesion and dark blue in the modulus) to the bulk uncoated glass bead (represented as purple in the adhesion and green/yellow in the modulus) for both adhesion and Young's

modulus. The uneven topography of the glass bead and the height difference between constituents is easily visualized using this representation of data.

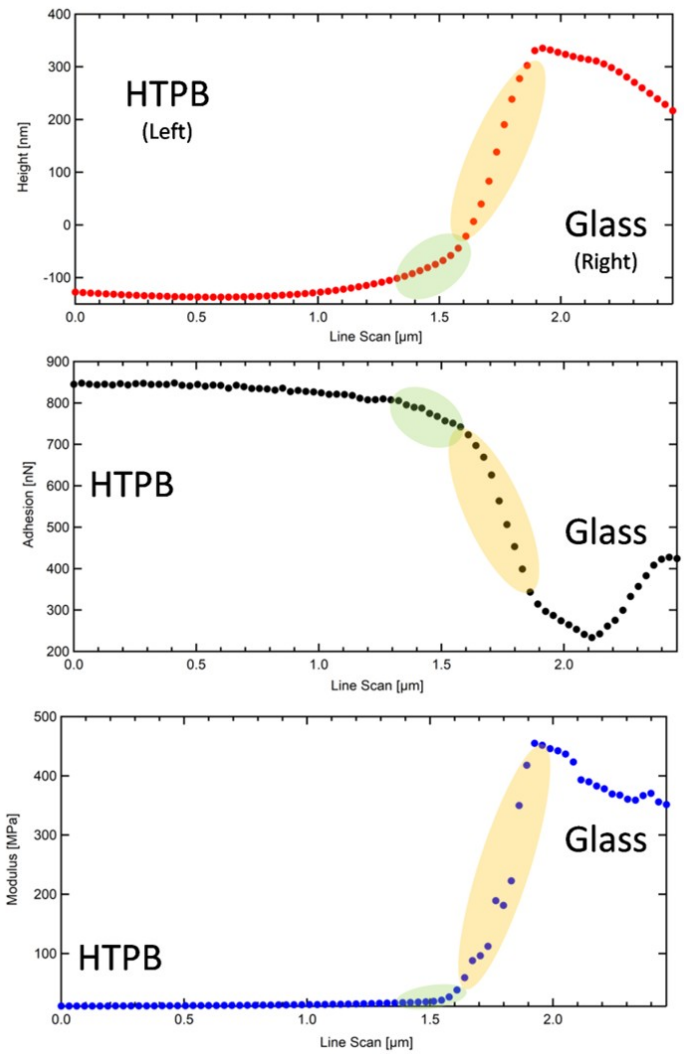

Fig. 10 Line scan across the interphase region of a different P4000-SC (4 wt. %) glass bead (bead A) showing the evolution in height (top, red circles), adhesion (middle, black circles), and modulus (bottom, blue circles) of the sample. The green highlighted areas show a "loosely bound interphase" region and the yellow highlighted areas show a "tightly bound interphase" region (see main text for explanation)

To represent the color gradient data from figure 9 graphically, a line scan (red line in 2D images of figure 10) was performed, allowing for the evolution of the height, adhesion, and Young's modulus to be plotted against the line scan distance, shown in figure 10.

Two distinct transition regions are recognized when analyzing the adhesion and modulus line scan for bead A (middle and bottom traces of figure 10, respectively). The bulk HTPB is a soft and compliant binder, which translates to a large adhesion value (∼850 nN) and a small modulus value (10s of MPa). As the tip moves from the bulk binder towards the coated glass bead A, the adhesion and modulus values begin to deviate from those observed in the bulk, which can be referred to as the 'loosely bound' interphase region (highlighted in green in figure 10). In this region—that spans from ∼530 nm to ∼190 nm away from coated glass bead A—the adhesion decreases ∼150 nN and the modulus increases ∼70 MPa. The change in height over this "loosely bound interphase" region is ∼110 nm. As the tip continues to move towards the coated glass bead A, there is another observable change in adhesion and modulus, highlighted in yellow in figure 10, that can be considered the "tightly bound interphase" region. From ∼190 nm away from coated glass bead A there is a steep drop in the adhesion value (an additional ∼320 nN) and an even more drastic increase in the Young's modulus (increasing ∼260 MPa) until the values

converge on the average bulk value of coated glass bead A. The height change for this "tightlt bound interphase" region is ∼260 nm. From these results, the total interphase width of the bead A in the P4000-SC (4 wt. %) sample is ∼ 530 nm.

Bead B from P4000-SC (4 wt. %) in the same cross section was investigated. A line scan was performed, showing evolution of the height, adhesion, and Young's modulus of Sigmacote glass bead B in HTPB in figure 11. Again, there are two distinct transition regions observed as the scan moves from bulk HTPB towards the embedded bead. Both the adhesion and modulus values of bulk HTPB remain consistent between scans (∼ 850 nN and 10s of MPa, respectively). However, we begin to see deviations from bulk behavior beginning ∼ 2.4 μm away from the glass bead. From ∼ 2.4 μm to 600 nm away from the bead, the adhesion drops ∼300 nN and the modulus increases ∼10 MPa over a height change of ∼140 nm in the "weakly bound interphase" region, highlighted in green in figure 11. From 600 nm away to the edge of the bead, we again observe a more drastic change in nanomechanical properties in the "tightly bound interphase" region highlighted in yellow. We observe a decrease in adhesion of ∼ 300 nN and an increase of ∼150 MPa in modulus across a ∼190 nm height change. From the results in figure 11, the total interphase width of the investigated bead in the coated glass bead and HTPB sample is ∼ 2.4 μm, a stark difference from the previously investigated bead in figure 10. The range of interphase widths measured using AFM for the beads in P4000-SC (4 wt. %) are summarized in Table 4.

Next, we investigate uncoated glass beads in the P4000 (4 wt. %) sample from the same cross section using the same methodology. figure 12 shows the evolution of the height, adhesion, and Young's modulus across the interphase region of the

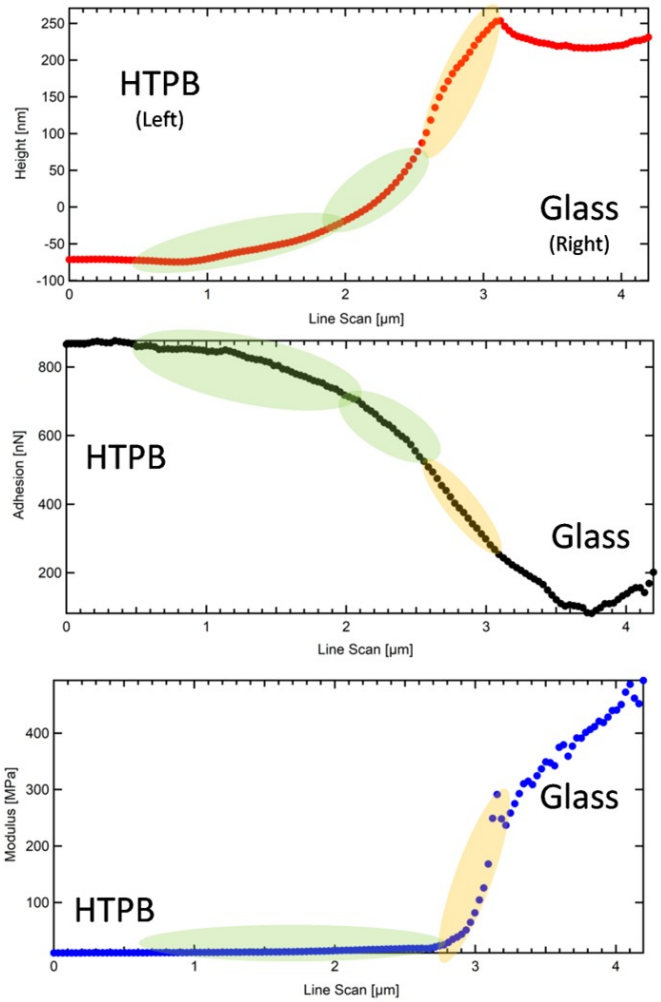

Fig. 11 Line scan across the interphase region of a different P4000-SC (4 wt. %) glass bead (bead B) showing the evolution in height (top, red circles), adhesion (middle, black circles), and modulus (bottom, blue circles) of the sample. The green highlighted areas show a "weakly bound interphase" region and the yellow highlighted areas show a "tightly bound interphase" region (see main text for explanation)

glass bead sample (denoted bead C). When analyzing this interphase region, we observe a deviation from bulk adhesion and modulus values beginning ∼440 nm away from the uncoated glass bead C. The adhesion value decreases ∼130 nN moving from ∼440 nm to ∼95 nm away from the interface, while the modulus increases ∼45 MPa. We again define this change from bulk properties as the 'weakly bound interphase' region, highlighted in green in figure 12. As the tip moves closer to the embedded bead, a second discernable change in the adhesion and modulus values is realized. From ∼95 nm away from uncoated bead C to the bead edge in the "tightly bound interphase" region, the adhesion value decreases ∼200 nN while the modulus increases ∼290 MPa. The total change in height over both the "weakly bound interphase" and 'tightly bound interphase" regions was nearly 450 nm, and the total interphase width is measured to be ∼ 450 nm for uncoated bead C in this sample.

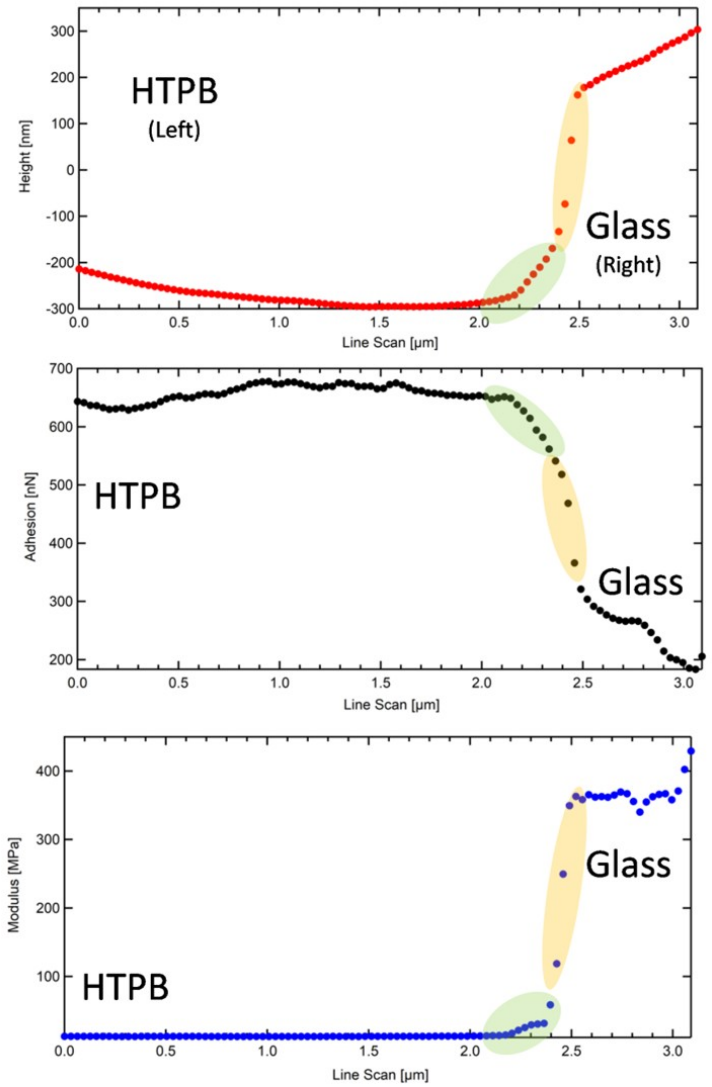

Fig. 12 Line scan across the interphase region of a P4000 (4 wt. %) glass bead (bead C) showing the evolution in height (top, red circles), adhesion (middle, black circles), and modulus (bottom, blue circles) of the sample. The green highlighted areas show a "weakly bound interphase" region and the yellow highlighted areas show a "tightly bound interphase" region (see main text for explanation)

Finally, we investigate another bead within the same cross section of the P4000 (4 wt. %) sample, defined as bead D. Deviations from the bulk adhesion and modulus values begin ∼ 2.3 μm away from uncoated glass bead D, shown in green in figure 13. From ∼2.3 μm to 400 nm away from the uncoated glass bead D the adhesion value decreases ∼250 nN while the modulus increases ∼11 MPa. Moving from 400 nm away to the edge of the uncoated bead D, there is another stark change in the adhesion and modulus values over a 350 nm height gradient. The adhesion value drops ∼230 nN and the modulus

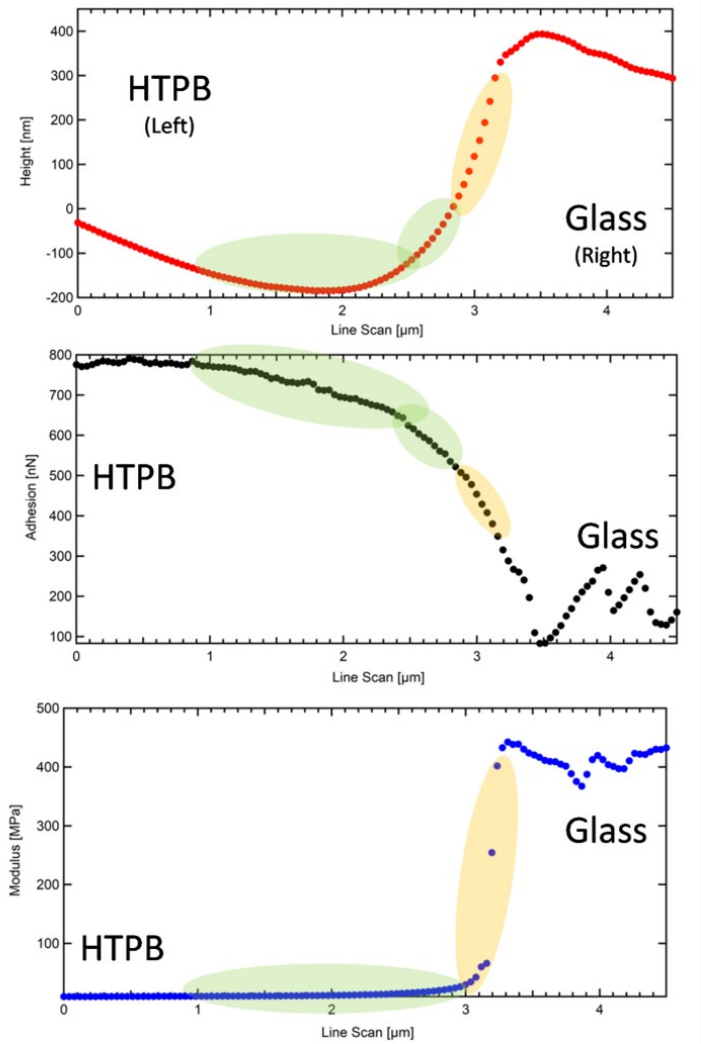

Fig. 13 Line scan across the interphase region of a different P4000 (4 wt. %) glass bead (bead D) showing the evolution in height (top, red circles), adhesion (middle, black circles), and modulus (bottom, blue circles) of the sample. The green highlighted areas show a "weakly bound interphase" region, and the yellow highlighted areas show a "tightly bound interphase" region (see main text for explanation)

increases ~380 MPa before both values plateau to the bulk values of the uncoated glass bead measured under the present conditions. The total interphase width measured for uncoated glass bead D in HTPB (over a large deviation in height over 500 nm) is ~2.3 μm, summarized in Table 4.

The results of the interphase width range for the 25–40 μm coated and uncoated glass beads in their respective samples are presented in Table 4. From this AFM study on embedded glass beads in HTPB, there is no observed consistency of the interphase width between beads of the same coating within a given cross section. Additionally, there is no observed difference in the interphase width between a coated glass bead and an uncoated glass bead in HTPB. We hypothesize the AFM results presented are dominated by a large height difference between constituents as opposed to a true representation of the interphase width. Nevertheless, it is important to highlight how AFM analysis of the interphase region is heavily influenced by the sample preparation method which, in turn, is heavily reliant on the binder and embedded particle chosen.

Additional bead sizes were not characterized at the time of this publication due to time constrains. Given the challenges cutting larger bead sizes, it is unlikely that the other samples would have yielded improved results. The variability of the interphase width measurements for the coated and uncoated P4000 (4 wt. %) samples, and a lack of data for other bead sizes prevents any correlation of the DMA results to interphase properties at this time. These challenges highlight a need to improve AFM sample preparation techniques for follow on investigations.

Table 4 Summary of interphase widths for P4000 (4 wt. %) and P4000-SC (4 wt. %) from AFM analysis

Glass Bead Coating	Average Particle Size (μm)	Interphase Width Range (μm)
Coated	16.75	0.5–2.4
Uncoated	14.35	0.4–2.3

Conclusions

This study investigated the particle-binder interphase regions in HTPB/glass bead composites with DMA and AFM and sought to correlate data between the two techniques. Glass beads were employed as the filler in a HTPB binder system and were varied from an average particle size of approximately 16 μm to 600 μm at a fixed volume % of filler. Glass beads were also coated with Sigmacote® to act as a shielding agent to weaken the particle-binder interaction strength.

DMA tan δ traces showed two clear peaks for most of the samples evaluated which indicated two separate relaxation process occurring within the material. The first peak at the colder temperature is from the T_g of the HTPB. The particle size and the coating on particles did not show any appreciable change to the T_g, but did result in differences in peak height. Investigation of the second tan δ peak did not explicitly prove any correlates to relaxation mechanism solely within the interphase, but these results support the argument that the interphase characteristics could affect the peak's size and shape. General trends in the tan δ vs temperature plots show that the particle size and Sigmacote® affect the peak heights. Outliers in the reported trends are suspected to be due to poor mixing during sample generation. Activation energy and interaction parameter calculations also suggest that changing the particle size and particle surface chemistry will affect the particle-binder interaction strength and subsequently, the interphase.

Correlating DMA data to AFM measurements was not possible at this time due to the challenges associated with AFM sample preparation. Due to the compliant nature of HTPB binder, the hardness of the glass beads, and the differences in the binder's and glass beads' respective coefficients of thermal expansion, it was difficult to achieve a pristine cross-section cut. AFM measurements do suggest the presence of "weakly bound interphase" and "tightly bound interphase" regions, however, there is a significant variability in the measurement. This highlights the need to improve sample preparation techniques to permit any correlation of AFM interphase measurements to DMA data in future work.

References

1. Bashir, M. A. (2021). Use of dynamic mechanical analysis (DMA) for characterizing interfacial interactions in filled polymers. *Solids*, *2*(1), 108–120. https://doi.org/10.3390/solids2010006
2. Adicoff, A., & Lepie, A. H. (1970). Effect of tensile strain on the use of the WLF equation. *Journal of Applied Polymer Science*, *14*(4), 953–966. https://doi.org/10.1002/app.1970.070140406
3. Azoug, A., Nevière, R., & Constantinescu, A. (2015). Molecular origin of the influence of the temperature on the loss factor of a solid propellant. *Propellants, Explosives, Pyrotechnics*, *40*(4), 469–478. https://doi.org/10.1002/prep.201400060
4. Bohn, M. A., Lemos, M. F., Mussbach, G. (2017*) Influence of concentration, type and particle size of fillers on the dynamic mechanical behaviour of elastomeric HTPB binder*. Fraunhofer ICT (International Annual Conference) 2017, Karlsruhe, Germany.
5. Gańczyk-Specjalska, K., & Magnuszewska, P. (2020). An analysis of the mechanical properties of HTPB-propellants using DMA. *Materiały Wysokoenergetyczne / High Energy Materials*, 81–91. https://doi.org/10.22211/matwys/0192
6. Tramell, J., Bohn, M., & Gerber, P. (2024, June 25-28) *Reproducibility and Applicability of Time-Temperature Superposition for Polymer Bonded Explosives Tested with Torsional Dynamic Mechanical Analysis*. 53^{rd} International Annual Conference of the Fraunhofer ICT on 'Energetic Materials – Structure and Properties', Karlsruhe, Germany.
7. Cerri, S., Bohn, M. A., Menke, K., & Galfetti, L. (2013). Aging of HTPB/AL/AP rocket propellant formulations investigated by DMA measurements. *Propellants, Explosives, Pyrotechnics*, *38*(2), 190–198. https://doi.org/10.1002/prep.201200186
8. Seyidoglu, T., & Bohn, M. A. (2020). Effects of four isocyanates and four plasticizers on the thermomechanical and tensile properties of hydroxyl-terminated polybutadiene elastomers and the effect of solid particle filling. *Journal of Applied Polymer Science*, *138*(18). https://doi.org/10.1002/app.50362
9. Tsagaropoulos, G., & Eisenberg, A. (1995). Dynamic mechanical study of the factors affecting the two glass transition behavior of filled polymers. similarities and differences with random ionomers. *Macromolecules*, *28*(18), 6067–6077. https://doi.org/10.1021/ma00122a011
10. Bohn, M. A., Musbach, G., & Cerri S. (2012, June 26-29) *Influences on the Loss Factor of Elastomer Binders and its Modeling*. 43^{rd} International Annual Conference of the Fraunhofer ICT on 'Energetic Materials – Synthesis, Characterisation, Processing', Karlsruhe, Germany. ISSN 0722-4087.
11. Li, R., Xu, Y., Zhang, K., Wu, Z., Ma, N., & Ouyang, X. (2024). A novel computational model based on molecular chain dynamics: Quantification and evaluation of interfacial interactions in polymer-based composite materials. *Composites and Advanced Materials*, *33*. https://doi.org/10.1177/26349833241309350

12. Lemos, M. F., Mussbach, G., & Bohn, M. A. (2017). Evaluation of filler effects on the dynamic mechanical behavior of HTPB-elastomer used as binder in exemplary composite formulations. *Journal of Aerospace Technology and Management*, *9*(3), 379–388. https://doi.org/10.5028/jatm.v9i3.795
13. Cheng, X.; Putz, K. W.; Wood, C. D.; Brinson, L. C. Characterization of Local Elastic Modulus in Confined Polymer Films via AFM Indentation. *Macromol. Rapid Commun.* **2015**, *36* (4), 391–397. https://doi.org/10.1002/marc.201400487.
14. Collinson, D. W.; Sheridan, R. J.; Palmeri, M. J.; Brinson, L. C. Best Practices and Recommendations for Accurate Nanomechanical Characterization of Heterogeneous Polymer Systems with Atomic Force Microscopy. *Progress in Polymer Science* **2021**, *119*, 101420. https://doi.org/10.1016/j.progpolymsci.2021.101420
15. Tian, C.; Chu, G.; Feng, Y.; Lu, Y.; Miao, C.; Ning, N.; Zhang, L.; Tian, M. Quantitatively Identify and Understand the Interphase of SiO2/Rubber Nanocomposites by Using Nanomechanical Mapping Technique of AFM. *Composites Science and Technology* **2019**, *170*, 1–6. https://doi.org/10.1016/j.compscitech.2018.11.020
16. Monclus, M. A.; Young, T. J.; Di Maio, D. AFM Indentation Method Used for Elastic Modulus Characterization of Interfaces and Thin Layers. *J Mater Sci* **2010**, *45* (12), 3190–3197. https://doi.org/10.1007/s10853-010-4326-6.Dynamic Mechanical Analysis Studies of the lnterphase - PING SENG CHUA
17. Bashir, M. A., Jakobsen, M. G., & Farstad, V. B. (2020). The effect of extender particle size on the glass transition temperature of model epoxy coatings. *Polymers*, *12*(1), 196. https://doi.org/10.3390/polym12010196
18. Hayeemasae, N., Soontaranon, S., & Masa, A. (2024). Comparative investigation of nano-sized silica and micrometer-sized calcium carbonate on structure and properties of natural rubber composites. *Polymers*, *16*(8), 1051. https://doi.org/10.3390/polym16081051
19. Robertson, C. G., Lin, C. J., Rackaitis, M., & Roland, C. M. (2008). Influence of particle size and polymer−filler coupling on viscoelastic glass transition of particle-reinforced polymers. *Macromolecules*, *41*(7), 2727–2731. https://doi.org/10.1021/ma7022364
20. Kubát, J., Rigdahl, M., & Welander, M. (1990). Characterization of interfacial interactions in high density polyethylene filled with glass spheres using dynamic-mechanical analysis. *Journal of Applied Polymer Science*, *39*(7), 1527–1539. https://doi.org/10.1002/app.1990.070390711
21. Lin, Cong-mei, Liu, S., Wen, Y., Liu, J., He, G., Zhao, X., Yang, Z., Ding, L., Pan, L., Li, J., & Guo, S. (2022). Sandwich-like interfacial structured polydopamine (pda)/wax/PDA: A novel design for simultaneously improving the safety and mechanical properties of highly explosive-filled polymer composites. *Energetic Materials Frontiers*, *3*(4), 189–198. https://doi.org/10.1016/j.enmf.2022.03.003
22. Lin, Congmei, Yang, X., He, G., Wen, Y., Qian, W., Liu, R., Liu, S., Gong, F., Zhang, J., Zeng, C., Yang, Z., Chen, R., & Guo, S. (2023). Mussel-inspired interfacial reinforcement of thermoplastic polyurethane based energetic composites. *Composites Science and Technology*, *232*, 109875. https://doi.org/10.1016/j.compscitech.2022.109875
23. Ashida, M., Noguchi, T., & Mashimo, S. (1985). Effect of matrix's type on the dynamic properties for short fiber-elastomer composite. *Journal of Applied Polymer Science*, *30*(3), 1011–1021. https://doi.org/10.1002/app.1985.070300311
24. Dossi, E.; Earnshaw, J.; Ellison, L.; Rabello Dos Santos, G.; Cavaye, H.; Cleaver, D. J. Understanding and Controlling the Glass Transition of HTPB Oligomers. *Polym. Chem.* **2021**, *12* (17), 2606–2617. https://doi.org/10.1039/D1PY00233C